

Contents lists available at [ScienceDirect](http://www.sciencedirect.com)

Aerosol Science

journal homepage: www.elsevier.com/locate/jaerosci

Compact multiplexing of monodisperse electrosprays

Weiwei Deng^a, C. Mike Waits^b, Brian Morgan^b, Alessandro Gomez^{a,*}^aDepartment of Mechanical Engineering, Yale University, 9 Hillhouse Avenue, New Haven, CT 06520, USA^bArmy Research Laboratory, 2800 Powder Mill Road, Adelphi, MD 20783, USA

ARTICLE INFO

Article history:

Received 27 March 2009

Received in revised form

9 July 2009

Accepted 10 July 2009

Keywords:

Electrospray

Microfabrication

Multiplex

Scaling law

ABSTRACT

Widespread application of the cone-jet electrospray has been hampered by the low flow rate at which the spray is dispersed, despite the unique ability of this device to disperse quasi-monodispersed particles over a phenomenal size range. Compact multiplexing, that is, with a high number of sources per unit area, is indispensable for dramatically increasing the throughput and reducing the cost per electrospray source. We demonstrate the successful operation of multiplexed electrospray systems with an unprecedented packing density of up to 11,547 sources/cm². The devices were fabricated and operated by implementing three criteria: (a) the extractor electrode configuration should be used to localize the electric field; (b) the viscous pressure drop acting on the liquid should dominate with respect to the electrostatic pulling force by the electric field; and (c) the electric field “driving” the droplets between the extractor electrode and the collector should be sufficiently intense to avoid reversal of the droplet motion near the extractor (satellite trapping). All devices showed excellent droplet size uniformity across the entire spray region, which indicates effective decoupling of the electrospray sources even for closely packed nozzles. The experimental results show that these design criteria provide effective and reliable guidelines for the successful design and operation of multiplexed devices from first principles, that is, based only on knowledge of the suitability of a liquid for electrospray dispersion and of the critical liquid properties such as surface tension, viscosity and electric conductivity. As a result, the design of these devices for a given application is achievable without costly trial-and-error microfabrication trials. This development opens the door for applications requiring flows from multiplexing 10⁶–10⁷ individual electrospray sources from industry-standard 12-in silicon wafers.

© 2009 Elsevier Ltd. All rights reserved.

1. Introduction

The electrospray (ES) is a liquid atomization technique relying solely on electric charging. The ES can be operated in several modes (Zeleny, 1917). One in particular is labeled cone-jet mode (Cloupeau & Prunet-Foch, 1989) because of the morphology of the liquid meniscus, referred to as the Taylor-cone (Taylor, 1964), at the apex of which a fine jet is anchored. The cone-jet ES offers not only the appealing feature of droplet monodispersity (Chen, Pui, & Kaufman, 1995; Fernández de la Mora, Navascues, Fernandez, & Rosell Llompart, 1990; Tang & Gomez, 1994b), but it is also stable, as opposed to most other electrostatic alternatives that are unsteady and often chaotic. The cone-jet ES has drawn increasing attention from the aerosol community mainly because of the phenomenal size range of particles it can produce, from molecular dimensions to hundreds of microns. The capability of easily producing monodisperse particles without clogging is unmatched by any other aerosol generation scheme, especially in the nanometric range.

* Corresponding author. Tel.: +1 203 432 4384; fax: +1 203 432 7654.

E-mail address: Alessandro.Gomez@yale.edu (A. Gomez).

Although the electrospray is in principle suitable to a variety of technological applications (Bailey, 1988; Jaworek & Sobczyk, 2008; Salata, 2005), Electrospray Ionization Mass Spectroscopy (ESI-MS) (Dole et al., 1968; Fenn, Mann, Meng, Wong, & Whitehouse, 1989) is the only practical application of the electrospray in widespread use. The key drawback that has hampered applications to other areas is the low flow rates at which the cone-jet mode can be established. Because the electrospray exhibits a monotonic dependence of droplet size on flow rate (Chen et al., 1995; Ganan-Calvo, Davila, & Barrero, 1997; Rosell-Llompart & Fernandez de la Mora, 1994; Tang & Gomez, 1996), for many potential applications such as microcombustion (Deng, Klemic, Li, Reed, & Gomez, 2007), insulin nanoparticle synthesis (Gomez, Bingham, De Juan, & Tang, 1998) and space propulsion (Romero-Sanz, Bocanegra, Fernández de la Mora, & Gamero-Castaño, 2003), the desired droplet size is so small that the corresponding low flow rates result in low throughputs that are far from practical. As a result, multiplexed electrosprays (MES) become indispensable.

MES has been pursued by various research groups with different approaches. On the basis of the ES source arrangement, these approaches fall in three categories: linear array, multi-jet mode and planar array. The linear array MES simply entails duplication of several capillaries operating in parallel by “brute force” (Rulison & Flagan, 1993), by etching of fused silica capillaries (Kelly, Page, Tang, & Smith, 2007), by soft lithography on PDMS (Kim & Knapp, 2001), or by silicon microfabrication (Kim, Guo, Yang, & Wang, 2007; Wang et al., 2007). These linear systems were demonstrated reliably with a limited number of sources (up to 20), although the linear packing density can reach 1000 sources/cm. The linear array adopted the traditional two-electrode configuration with the ground plate at a considerable distance from the linear array, which requires the space charge to be insignificant. Otherwise, the sprays become unstable, for reasons to be discussed later.

The multi-jet mode entails stabilizing a number of electrosprays on the circumference of the tube outlet through which a common liquid is pumped. When the electric field near the cone of the ES is sufficiently intense, the single jet may split into two or more jets (Cloupeau & Prunet-Foch, 1990). Duby, Deng, Kim, Gomez, and Gomez (2006) reported on a novel approach to multiplexing based on the multi-jet mode. By precisely machining some sharp grooves at the outlet of the atomizer, these authors were able to intensify the electric field at discrete points around its perimeter. Then, several cone-jets were simultaneously anchored at these groove edges and a stable mode of operation was identified over several hundreds of volts and a broad range of flow rates. Most importantly, as long as the geometry was accurately reproduced from groove to groove, the droplets generated did not vary significantly in size from spray to spray. This simple, compact, inexpensive and versatile MES system is well suited for multiplexing the order of tens of sources, and it was successfully used as a jet fuel atomizer in a small power system (Gomez, Berry, Roychoudhury, Coriton, & Huth, 2007).

Planar MES systems have been implemented with nozzles made by laser etching (Tang, Lin, Matson, Kim, & Smith, 2001) and with an array of holes by conventional drilling (Bocanegra, Galán, Márquez, Loscertales, & Barrero, 2006), achieving packing densities of ≤ 100 sources/cm² and a number of sources < 40 . The hole system may have limited versatility because it relies on the liquid (de)wetting the outlet surface, which either applies to certain liquid-surface pairs or requires special coatings. The dewetting is necessary to ensure that the liquid pumped through the multiple openings accumulates locally at the openings for it to be drawn into parallel cone-jets rather than spreading over the entire surface.

It is clear that a high level of multiplexing and compactness of the MES are mutually exclusive goals unless one adopts (silicon-based) microfabrication that can easily achieve feature sizes on the order of 1 μm . Deng, Klemic, Li, Reed, and Gomez (2006, 2007) demonstrated a microfabricated array of up to 331 sources with a packing density of 250 sources/cm². A high multiplexing level was also reported by Velásquez-García, Akinwande, and Martínez-Sánchez (2006) with an array of 1024 ES emitters of externally fed ionic liquid having a packing density of 2500 sources/cm². The ionic liquid, driven by surface tension, has a large surface exposed to the surroundings; therefore its evaporation rate will be larger by comparison than traditional channel flow. Consequently the approach of Velásquez-García et al. (2006) may not be suited for highly volatile fluids and may hamper the delivery of the flow rate in a controlled fashion, especially if the flow rate per hole is very small.

For a MES system, a high packing density is often desirable for three reasons. First of all, integrating more sources per unit area can reduce the cost per nozzle because the average microfabrication cost scales with wafer area. Secondly, smaller nozzles are essential in several applications. For example, in electrospray space propulsion, the diameter of the Taylor-cone needs to be $\sim 10 \mu\text{m}$ to suppress solvent evaporation (Bocanegra, De La Mora, & Gamero-Castao, 2004). Another example is the ESI-MS source operated in the nano-spray regime, in which the outer diameter of the nozzle is typically 30 μm or less. Lastly, denser packing of ES sources makes the neighboring sprays “merge” more quickly, therefore a homogenous droplet cloud can be produced within a shorter travel distance, which can make potential applications fit within a compact volume.

In this article, we report on the development and performance of MES devices having a planar nozzle array and unprecedented packing densities reaching 11,547 sources/cm². Importantly, we verified excellent droplet size uniformity from nozzle to nozzle as a result of following three design criteria that were initially proposed in Deng et al. (2006, 2007) and are now substantiated over a broad parameter space. As a result, the design of these devices for a given application is achievable from first principles, without costly trial-and-error microfabrication trials.

2. Experimental approach

The centerpiece of the MES system is a distributor chip with planar nozzle arrays arranged in a hexagonal pattern. The number of nozzles on the chip is 1, 7, 19, 61, 91, 331, or 1027. All chips were microfabricated at the US Army Research Laboratory (ARL) using a series of photolithography and tailored Deep Reactive Ion Etch (DRIE) processing of silicon wafers. The typical

Table 1

Key nozzle geometric features of the MES devices: OD—nozzle outer diameter, ID—nozzle inner diameter, H —nozzle protrusion, P —distance between two neighbouring nozzles and PD—packing density.

Device code name	OD (μm)	ID (μm)	H (μm)	P (μm)	PD (sources/cm ²)
M210	210	60	475	675	253
M90	90	45	230	300	1283
M60	60	30	156	200	2887
M30	30	15	81	100	11,547

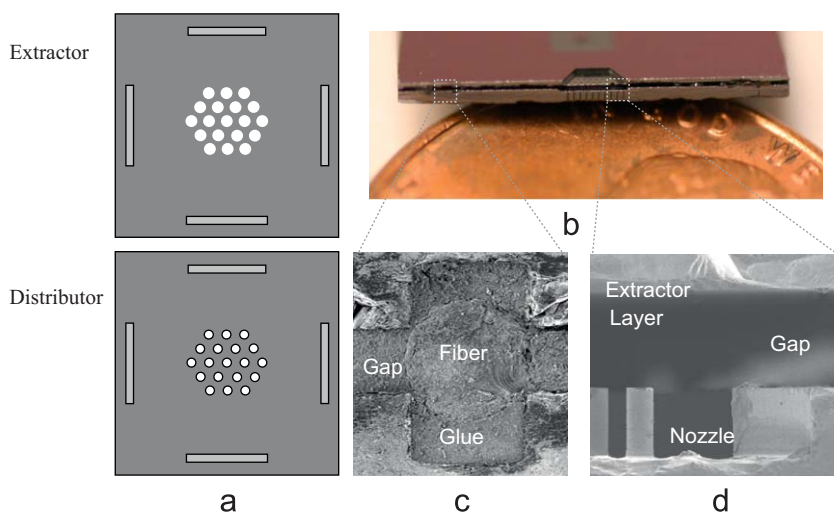


Fig. 1. Device alignment technique: (a) schematic of the distributor chip and extractor chip with four alignment trenches etched in them; (b) photograph of the cross cut of the assembled distributor/extractor pair placed next to a penny as a reference scale; (c) SEM micrograph of the cross section of the alignment point showing the trench, fiber, glue and gap; and (d) SEM micrograph of the side view showing the nozzle, gap and extractor layer.

microfabrication flow and developed microfabrication processes were documented in Deng et al. (2006) and Waits et al. (2008). The extractor was also fabricated in silicon using similar microfabrication processes. We made devices with four different packing densities of 253, 1283, 2886, and 11,547 sources/cm², respectively. Table 1 summarizes the key geometric features of the MES devices.

Manual alignment of the distributor chip and the extractor becomes extremely challenging as the nozzle OD is $< 100 \mu\text{m}$. Slight misalignment between the nozzle and the extractor hole may cause the jet/spray to discharge asymmetrically, hit the extractor and cause flooding. Furthermore, the accumulated liquid between the extractor and the nozzle array will lead to an electrical short between the two components. Although state-of-the-art conventional bond alignment techniques can achieve an alignment tolerance of $1 \mu\text{m}$, optical access to the cone region and cleaning flexibility are limited in the testing stage. To address this problem, we developed a novel alignment and bonding technique to assemble the two components of the MES unit, the nozzle array and the extractor electrode, with high alignment and gap precision (Waits et al., 2008). This technique used optical fibers with a diameter of $250 \mu\text{m}$ for device M90 and $125 \mu\text{m}$ for devices M60 and M30. The fibers rest in opposing trenches etched into the two components and sandwiched by them, eliminating the need for specialized alignment equipment. The tight diameter tolerance of the optical fiber dimension enables both alignment and gap control by lithographically tailoring the width of the alignment trenches, and the circular fiber cross section provides self-centering alignment between the two stacked chips. In addition, the optical fiber is electrically insulating and capable of holding off the applied extractor–distributor potentials (on the order of kV). As shown in Fig. 1a, four identical alignment trenches were defined and fabricated on both the distributor and the extractor. The trenches are first filled with silicone glue, and then the optical fiber is placed into the alignment trench. Next, the distributor and the extractor die are aligned by gently sliding one piece with respect to the other until the optical fibers are exactly sandwiched between the alignment trenches (Fig. 1c), and a precise gap is automatically achieved (Fig. 1d).

The alignment accuracy and gap precision were measured using an optical profilometer. The alignment accuracy was evaluated by how centered the nozzle is to the extractor opening when looking from the top of the extractor. The distance between the edge of the circular opening above the nozzle in the extractor and the edge of the nozzle is compared on opposing sides and in multiple positions to obtain estimates of the lateral misalignments. The measurements showed alignment to within $1 \mu\text{m}$. After accounting for the measurement error of the interferometric profilometer and degradation of the circular shape during the fabrication processes, we estimate alignment accuracy on the order of $0.5 \mu\text{m}$.

The spray can be visualized by a laser beam, which was first expanded and then focused by a 300 mm cylindrical lens into a laser sheet. The orientation of the laser sheet could be either parallel or perpendicular to the distributor surface, and the

perpendicular orientation allowed for the visualization of spray plumes. For devices M210, M90 and M60, it is possible to observe the liquid cones from each nozzle through a high power optical microscope between the distributor and the extractor under strong back illumination. For device M30, the reduced gap prevented us from directly observing the Taylor-cones.

We tested two liquids with different conductivities: pure ethanol with a measured conductivity of 1.3×10^{-5} S/m and ethanol doped with 5 PPM by weight of an ionic liquid, 1-ethyl-3-methylimidazolium ethylsulfate, with a measured conductivity of $K = 1.0 \times 10^{-4}$ S/m. The liquid was pumped continuously into the reservoir by a syringe pump with different syringe sizes to ensure that the plunger would be displaced at a reproducible and accurate speed. Droplet sizes were measured by an optical fiber Phase Doppler Particle Analyzer (PDPA, TSI) capable of measuring simultaneously the droplet size and two velocity components from the scattering of a frequency-modulated Argon Ion laser beam (Coherent, Inc).

3. Design criteria

An ideal MES system should reproduce the ES exactly from source to source. In reality, when ES sources are packed densely together, they will interfere with each other both in terms of electrostatics and fluid mechanics. A successful design needs to minimize the two types of interference and essentially decouple the ES sources. Moreover, excessive space charge may also hinder sustainable device operation. In this section, we briefly summarize the design criteria that address these problems (Deng et al., 2006, 2007) and add some additional information.

3.1. Use of the extractor electrode configuration to localize the electric field

To minimize variation in the electric field from source to source, an extractor must be brought very close to the source with a gap comparable with the source diameter and pitch. The extractor not only localizes the electric field, but also shields the Taylor-cones from the highly charged spray cloud. Fig. 2 shows a typical electrode arrangement, in which the distributor electrode and extractor electrode are separated by a spacer/insulator, and a collector electrode is positioned 2–10 mm away from the extractor. The region between the liquid distributor chip and the extractor is named the jet-forming region, and the space between the extractor and the collector is defined as the spray region. The electrodes were maintained at different potentials to achieve the desired electric fields with $V_1 > V_2 > V_3$ and V_3 typically being ground, but negative values are also possible. This extractor electrode configuration is virtually indispensable for multiplexing configurations.

3.2. Dominance of viscous force on the liquid

The extractor cannot completely eliminate the electric field non uniformity, especially at the edge of the array. This non uniformity causes a non-uniform electrostatic pull of the liquid, which in turn results in unevenly distributed flow rates, with typically larger flow rates and droplet sizes near the periphery of the array. One solution to this problem is to make the viscous pressure drop across each nozzle dominant, typically one order of magnitude larger than the electrostatic stress. The viscous pressure drop should also be uniform from source to source, which can be easily achieved by appropriately sizing the nozzle inner diameter of each source and relying on the high spatial resolution of microfabrication and its capability of reproducing geometric features with high accuracy.

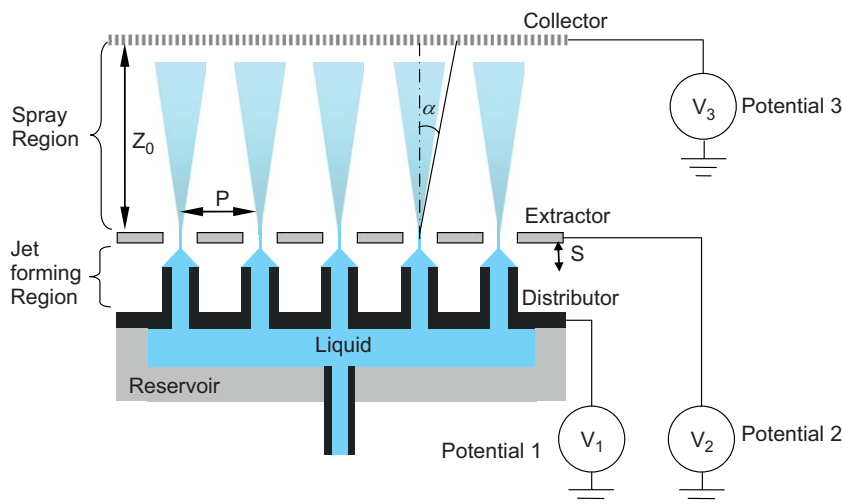


Fig. 2. Three-electrode configuration for the MES device with planar nozzle array.

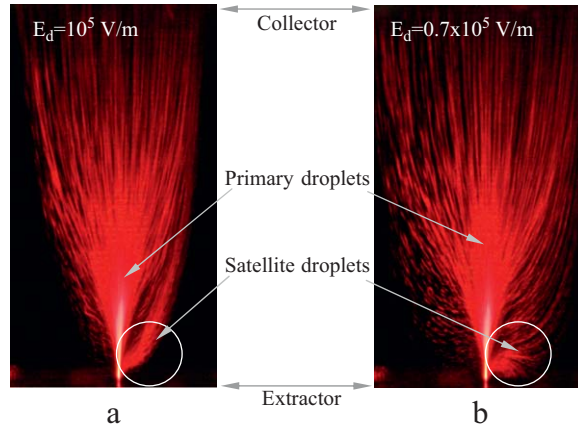


Fig. 3. The effect of the driving field on satellite droplets: (a) the satellite droplets (circled area) fly toward the collector under a sufficiently intense driving field, whereas in (b) a portion of the satellites fly back to the extractor (circled area) because of the reduced driving field.

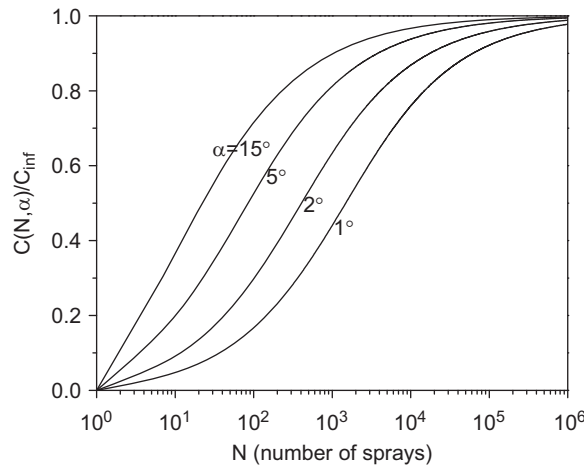


Fig. 4. Proportionality constant of the scaling law as a function of the number of sprays.

3.3. Sufficiently intense driving field to avoid satellite trapping

MES operation failure is often caused by the intense space charge of the system (Deng & Gomez, 2007). As the space charge intensity increases, the spray cloud tends to repel the droplets exiting the extractor and causes them to reverse their path, accumulate on the extractor, leading to flooding and termination of the MES operation. Fig. 3 shows details of the process that can be avoided by increasing the intensity of the driving electric field. The satellite droplets are usually more vulnerable to the space charge electric field because of their smaller inertia and shorter stopping distance. This phenomenon of satellite trapping represents the limiting electrostatic factor preventing proper MES operation. To avoid it, the driving field between the extractor and the collector (see Fig. 2), E_d , needs to be kept above a critical value, E_{cr} , and obviously below the breakdown threshold, E_{bd} , of the environment in which the ES is dispersed, that is $E_{bd} > E_d > E_{cr}$. This minimum critical value is determined by

$$E_{cr} \approx \tau \frac{I}{A} C(N, \alpha), \tag{1}$$

where τ is the primary droplet residence time (on the order of 1 ms) between extractor and collector, I/A is the current emitted per unit area and $C(N, \alpha)$ is a coefficient that depends on N (number of ES sources) and α , the semi-angle of the conical region that is available to each ES to disperse. α , in turn, depends on the extractor–collector separation Z_0 and the inter-nozzle distance, P , as $\alpha = \tan^{-1}(P/2Z_0)$. α is a measure of the contribution of each ES to the overall space charge field: a more slender angle results in a less significant contribution from each ES to the overall space charge field. On the basis of a simple but effective line-of-charge model (Deng & Gomez, 2007), we can estimate the minimum driving field by plotting $C(N, \alpha)$ in Fig. 4 as a function of N . Several curves are shown as a function of α . All $C(N, \alpha)$ approaches $C_{inf} = \sqrt{3}/2\epsilon_0$ as N approaches infinity, where ϵ_0 is the permittivity in

vacuum. One can insure that the approximate equality is satisfied by varying I/A , through changes in flow rate, liquid conductivity and nozzle pitch, and τ , by changing Z_0 , and the droplet velocity, via changes in the electrostatic and/or aerodynamic forces acting on the droplets.

In summary, these three design criteria enable end users to estimate the maximum packing density (ES sources per unit area) that a given fluid with known physical properties can be delivered with uniform droplets of a specified size. As a result, the traditional trial and error methodology that has characterized progress in this field is eliminated, which is very advantageous in view of the significant cost associated with microfabrication at the prototype stage.

4. Results and discussion

4.1. Evaluation on the effectiveness of decoupling ES sources

As discussed earlier, each ES source in an ideal MES device should be completely decoupled in terms of the electric field as well as flow field interference. Perfect decoupling can never be achieved, but nonetheless good uniformity of flow rate and minimization of space charge can be accomplished by applying the design criteria discussed earlier. One way to evaluate the effectiveness of decoupling is to measure the droplet size distribution across the device. Among all devices tested, M210 is best suited for this evaluation purpose for two reasons. First, M210 has a modest packing density, and the distance between two neighboring ES is $675 \mu\text{m}$, which is significantly larger than the probe volume length ($\sim 100 \mu\text{m}$) of the PDPA. As a result, it allows for diagnosis of the behavior of each individual ES with the PDPA with ease. Second, the relatively large inter-nozzle distance ensures that neighboring ES remain well separated 2.5 mm downstream from the extractor, which is as close as the PDPA probe volume can be positioned to the extractor.

Fig. 5 shows the performance data of a 91-nozzle M210 device with pure ethanol as the working liquid. The average flow rate is 0.6 cc/h per source, and the total flow rate is 54.6 cc/h . At each of the 11 ES along the diagonal of the hexagonal array, the average droplet diameter \bar{D}_i is measured. To better understand the data shown in Fig. 5, we define two relative standard deviations (RSD) as follows: the first, RSD_i , is the relative standard derivation of droplet diameter as measured within the i th ES; the second, RSD_o , is the overall relative standard derivation of the average droplet diameter of all measuring points, i.e.,

$$RSD_o = \frac{1}{\bar{D}} \sqrt{\sum_{i=1}^N (\bar{D}_i - \bar{D})^2 / (N - 1)},$$

where $\bar{D} = \sum \bar{D}_i / N$ is the droplet size averaged over all measuring points.

In Fig. 5, all of the RSD_i are < 0.09 , attesting to good monodispersity and suggesting they are all operated in cone-jet mode. More importantly, RSD_o is as small as 0.02 , which suggests that all ES are virtually identical. The result implies that, indeed, the viscous drag in the nozzle is the dominant force controlling the flow-rate through each nozzle, non-uniformities in the electric field being of secondary importance, and that the flow-rate is uniformly distributed. Additionally, the system exhibited easy start-up and turn-down, without any hysteretic behavior that has been described in Deng et al. (2006). Additional experiments with a distributor of 331 nozzles revealed comparable trends. Therefore, we conclude that the closely packed ES sources are effectively decoupled once the design criteria are applied.

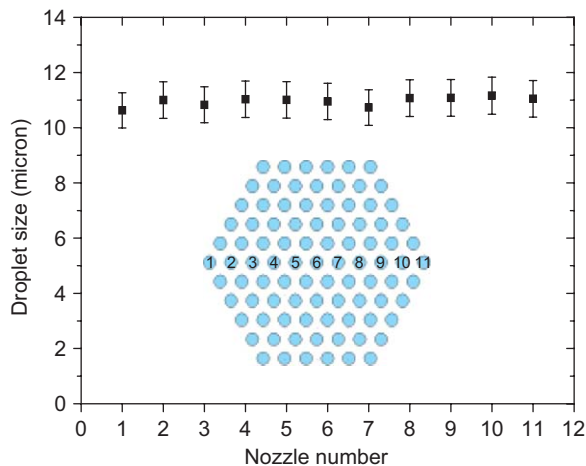


Fig. 5. Droplet size distribution of the 11 ES along the diagonal of a 91-nozzle M210 device.

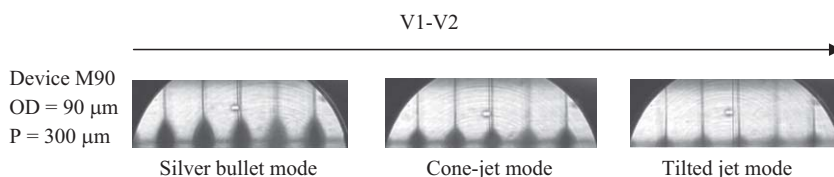


Fig. 6. Cone and jet visualization under microscope of M90 (1283 sources/cm²) in operation.

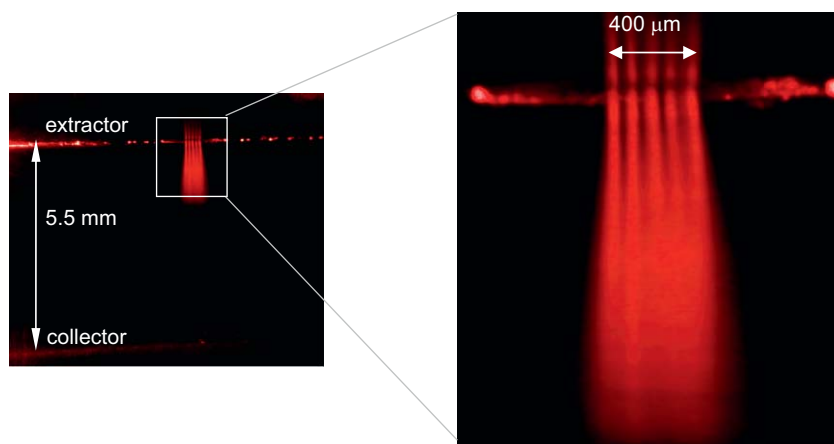


Fig. 7. Spray visualization of a 19-nozzle multiplexed electro spray system (M30) with a packing density of 11,547 sources/cm².

4.2. Performance of MES with high packing densities

After the design criteria were successfully validated with device M210, we designed and fabricated three new devices, M90, M60 and M30 with packing densities of 1283, 2887 and 11,547 sources/cm², respectively.

For M90 and M60, we were able to observe the Taylor-cones established at the tip of the nozzle through a high power microscope with a field of view of $\sim 800 \mu\text{m}$. Fig. 6 shows the typical cone and jet visualization photographs of M90. Notice that both the extractor and distributor have shiny surfaces, consequently each electro spray has multiple reflected images between the extractor and the nozzle chip. The typical range of potential bias ($V_2 - V_1$) is several hundred volts. For example, the bias range for M90 was from 0.81 to 1.26 kV. At the low bias end, the cone was elongated resembling the so-called silver bullet mode (Chen et al., 1995) (Fig. 6, left image). When the bias voltage was lowered below the low bound, the dripping mode regime was established, which is undesirable because it usually generates large and polydispersed droplets. In the mid-range of the bias range, the cones appeared to be well defined and the jets were parallel to the nozzle axis (Fig. 6, center image). At the upper limit of the range, the cones were significantly shrunk and not asymmetric anymore. Consequently, the jets were tilted (Fig. 6, right image), with risk of hitting the sidewall or even the surface of the extractor and causing device flooding. Device M60 behaved similarly to M90. Moreover, the response of each individual ES source to the change of voltage is consistent with the well-known single electro spray behavior.

The Taylor-cone from M30, with a $30 \mu\text{m}$ nozzle outer diameter and a $100 \mu\text{m}$ inter-nozzle distance, was not readily visible even with the aid of the microscope because of the dramatically reduced gap that limited optical access. However, we could visualize the sprays between the extractor and the collector. Fig. 7 shows the image of five electro sprays along the diagonal of the hexagonal array under Helium–neon laser sheet illumination. The width of the laser sheet was also focused to increase the illumination power density, and it does not cover the complete spray along the vertical direction, leaving some dark area downstream which does not indicate that the droplets are fully evaporated. The sprays expanded and became indistinguishable at $\sim 500 \mu\text{m}$ below the extractor. Strictly speaking, we cannot claim that sprays of homopolarly charged droplets merge because Coulombic repulsion is always at work. However, Fig. 7 clearly shows that the volume devoid of droplets downstream of the sources vanished, that is, the individual electro sprays grazed each other.

We also measured the droplet diameter in M90, M60 and M30. We were not able to take data for each individual spray source because the laser probe volume could not access the region where the sprays are fully separated. Instead, we made a transverse scan with a constant step of $100 \mu\text{m}$ (for M60 and M30) and $200 \mu\text{m}$ (for M90). The results are shown in Fig. 8. The RSD_0 for the three devices are 0.02, 0.02 and 0.04, respectively, all of which are comparable with that of device M210. These results also confirm that the MES devices generated homogenous droplets across the entire spray. However, at certain measurement points the RSD_i could be as high as 0.16, which is noticeably larger than those reported in Fig. 5 (< 0.09). The explanation is that the

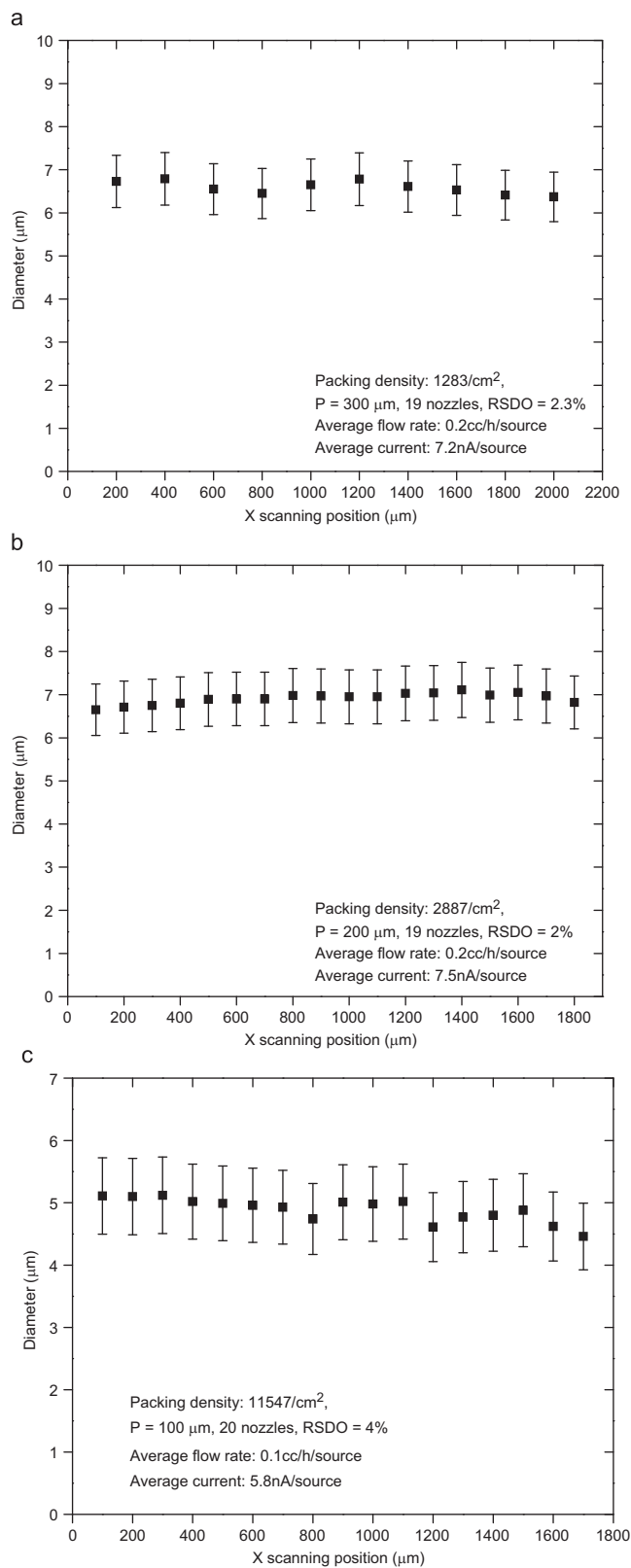


Fig. 8. Droplet size distribution measurements of MES devices with packing densities of: (a) 1283 sources/cm²; (b) 2887 sources/cm²; and (c) 11,547 sources/cm².

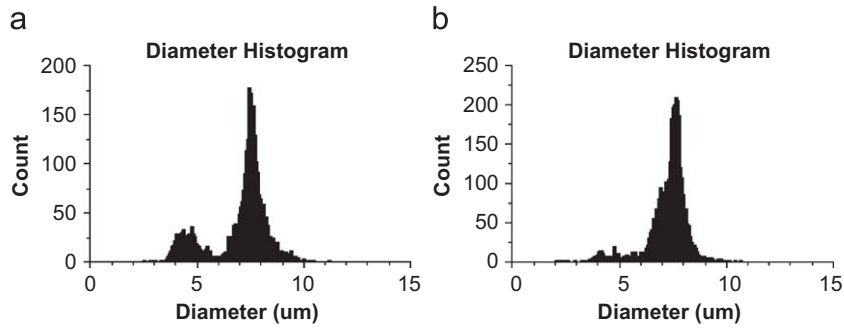


Fig. 9. PDPA diameter histograms measured at two positions with the sprays generated by M90: (a) bimodal distribution showing both primary droplets and satellites; and (b) distribution with the peak of satellites significantly suppressed.

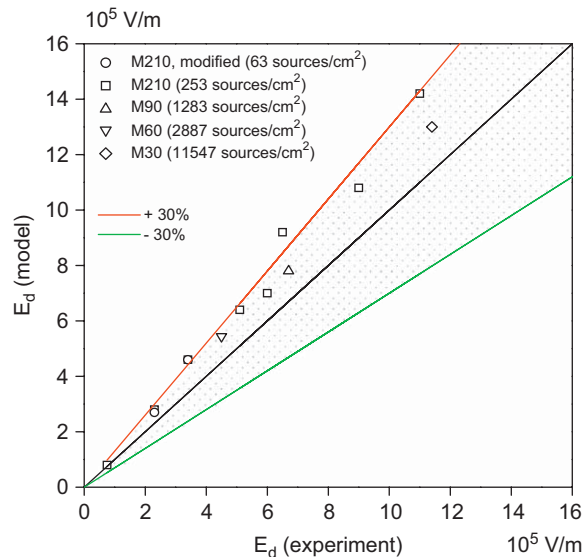


Fig. 10. Comparison between the modeled driving field, using the line of source approximation and some algebraic simplifications, versus the experimental values.

measurements were not always performed in the ES center where only primary droplets exist. When that is the case, the probe volume may sample a mixture of both primary droplets and satellites that are formed at breakup as a result of nonlinearities, as documented in Tang and Gomez (1994b). This limitation inevitably deteriorates the RSD_i . Fig. 9 shows two typical droplet diameter histograms. Fig. 9a shows two peaks: one corresponding to primary droplets and the other to the satellites. Both peaks, if analyzed separately, have $RSD_i < 12\%$, a value that is indicative of good monodispersity. In Fig. 9b, as the measuring point is closer to the center of one particular ES, the presence of satellites is significantly suppressed, leaving the primary droplets peak dominant in the histogram. Nevertheless, Fig. 8 again indicates an effective decoupling of ES sources for MES devices with very high packing density up to $O(10,000)$ sources/cm². Two additional remarks are in order: first, the size distribution measured by the PDPA may overestimate the standard deviation, as a result of an artifact associated with the trajectory of the droplet across the probe volume (Schaub, Alexander, & Barton, 1994); second, as remarked in Tang and Gomez (1994b), despite the presence of the satellites, the bulk of the flow rate, on the order of 90%, is dispersed in primary and virtually uniform droplets.

4.3. Verification of the space charge scaling law over a broad parameter range

The newly designed and fabricated devices, M90, M60 and M30 provide us the opportunity of further verifying if the space charge scaling law, $E_d > \tau(I/A)C(N, \alpha)$ (Deng & Gomez, 2007), holds over a relatively broad parameter range. With the complete collection of devices, we were able to vary the key parameters by more than one order of magnitude: the inter-nozzle distance P by a factor of 13.5, from 100 μm of M30 to 1350 μm of a modified M210 with every other nozzle clogged; I/A by a factor of 90; the number of sources by a factor of 47, from 7 to 331; and the residence time by a factor of 10. Fig. 10 shows the driving field

as modeled using the line of source approximation and some algebraic simplifications, E_d (model) vs. E_d (experiment) from the experimental values. Perfect agreement would yield a 45° bisetrix, as indicated by the solid black line. The shaded area covers an error of $\pm 30\%$ with respect to the bisetrix. The scaling law tends to overestimate the driving field systematically for three major reasons: (a) it is a conservative estimate because the inertia of the satellites was neglected; (b) primary droplets may be accelerated by the intense driving field and the effective charge per unit length of the line-of-charge is not uniform but would decrease; and (c) the sprays repel each other further downstream, so that the volume charge density decreases and the space charge field is weakened. The relatively modest error (typically $\leq 30\%$), the simplicity of its functional form, its validation over a broad parameter range and its conservative nature, since it systematically overestimates the necessary driving field, suggest that the space charge scaling law is an effective and safe tool to guide the design and operation of MES devices.

5. Further scale-up and potential applications

Despite the promise of high-density multiplexing, the ES is not envisioned to be used for mass production of raw materials, such as TiO₂ produced in tons by the pigment industry, or for fuel dispersion in a gas turbine. It is probably suited for high value-added applications, such as those of relevance to the pharmaceutical industry or the electronic industry, and niche markets, such as those of the highly specialized ion propulsion or small-scale combustion.

It should also be obvious that if it were desirable to have a multimodal distribution with the simultaneous dispersion of droplets of distinct sizes, this goal is easily achievable by microfabrication: through appropriate masks, nozzles of different diameters could accommodate different flow rates for a constant pressure head, and, consequently, generate droplets of different sizes, in view of the monotonic dependence of droplet size on flow rate. If the liquid distributor design is not made significantly more complex and the pressure drop, Δp , is maintained constant across all nozzles, the difference in diameter should be modest since the distribution of flow rate across nozzles will become uneven, as the flow rate through each nozzle scales as $\Delta p(ID)^4$.

Using microlithographic fabrication, one may multiplex by several orders of magnitudes with the same nozzle density and identical fabrication process as demonstrated here. For example, maintaining the same packing density of M90 or M30 for a standard 12-in wafer would realize 10^6 – 10^7 parallel sources in a relatively small footprint. This consideration may shed light on applications that can benefit from this development. In Table 2 we list some examples based either on known needs or maximum feasible throughput with the type of application, the desirable droplet/particle size, the flow rate per nozzle, the desirable total flow rate and the level of multiplexing in columns one through six, respectively. The first five are applications that have been demonstrated either at the level of a single electrospray or with a modest level of multiplexing. We conclude with an estimate of the feasibility of the technique in a less exotic and ubiquitous application: the internal combustion engine. Intense research is focused on the development of a homogenous charge injection compression ignition (HCCI) engine that is predicated on burning lean and well-mixed mixtures of fuel and oxidizer. Good atomization is key to achieving this goal. The multiplexed system could accommodate the necessary flow rate per cylinder, estimated at 2000 cc/h for concreteness, with $M = 5 \times 10^3$, which can be dispersed in $O(1)$ cm² footprint, which is compatible with the dimensions of the cylinder bore. Monodispersity is unlikely to be desirable for such an application since an ideal spray must have some combination of large droplets for good penetration into the oxidizer and small droplets for rapid vaporization. In such a case, an injector with a multimodal distribution tailored to the application can be microfabricated, through appropriate masks producing nozzles of different diameters.

In applications in vacuum such as space propulsion by ES operated in the ionic regime (Romero-Sanz et al., 2003), the space charge does not impose severe problems because the extremely high ion velocity of $\sim 10^4$ m/s ensures very low line-of-charge density. Moreover, the breakdown threshold E_{bd} would not be a cause for concern. However, for the others, there may be conditions under which severe space charge limitations set in, which may have to be mitigated or altogether circumvented. For example, for nanoparticle synthesis, the flow rate may have to be severely restricted to ensure the generation of very small droplets, which typically requires highly conductive solutions. This constraint results in large currents and limits the density of the MES sources in accordance with the approximate equality (1). To have a large level of multiplexing and maintain a small footprint, one may wish to mitigate any space charge problem by partially neutralizing the droplets using an array of microfabricated tips of opposite polarity, suitably positioned downstream, to generate electrons. The goal would be to partially neutralize the positively charged droplets, leaving just enough charge to prevent coalescence and enhance deposition. A similar scheme was used in

Table 2

Comparison between the flow rate of a single electrospray and the flow rate required by some potential applications.

Application	Preferred droplet size	Q_{single} (cc/h) (flow rate for a single ES)	Q_{total} (cc/h) (preferred total flow rate)	$M = Q_{\text{total}}/Q_{\text{single}}$ multiplexing level
200 W jet fuel microcombustor (Deng et al., 2007)	$\sim 10 \mu\text{m}$	0.4	6	50
CPU spray cooler (Deng & Gomez, 2008)	$< 25 \mu\text{m}$	2	100	50
LC/ESI-MS (Kelly et al., 2007)	N/A	1.2×10^{-3}	0.12	10^2
Space propulsion (Romero-Sanz et al., 2003)	Ions	2.4×10^{-6}	2.4×10^{-3}	10^3
Insulin nanoparticle synthesis (Gomez et al., 1998)	100 nm	2×10^{-2}	800 ^a	4×10^4
HCCI engine	$\sim 10 \mu\text{m}$	0.4	2000	5×10^3

^aAssuming a production rate of 10 g/h.

earlier work on ES applications to drug inhalation (Gomez, 2002; Tang & Gomez, 1994a). No experiments have been reported to evaluate the effectiveness of this approach for large currents and high level of multiplexing.

6. Conclusions

An experimental study was conducted on the feasibility of implementing ultra-dense multiplexing of the electrospray and yet preserving size uniformity of the generated droplets. Principal conclusions follow.

- We demonstrated the successful operation of multiplexed electrospray systems with packing density up to $O(10,000)$ sources/cm², the highest value that has been reported to date.
- All devices were fabricated and operated by implementing three criteria: (a) the extractor electrode configuration should be used to localize the electric field; (b) the viscous pressure drop acting on the liquid should be dominant with respect to the electrostatic pulling force by the electric field; and (c) the electric field “driving” the droplets between the extractor electrode and the collector should be sufficiently intense to avoid reversal of the droplet motion near the extractor (satellite trapping).
- All devices showed excellent droplet size uniformity across the entire spray region, which indicates effective decoupling of the ES sources, that is, each electrospray performs as if it were isolated from the others even for closely packed nozzles.
- The experimental results show that these design criteria are effective and reliable guidelines for a successful design and operation of planar nozzle MES devices from first principles, that is based only on knowledge of the suitability of a liquid for electrospray dispersion and of the critical liquid properties (surface tension, viscosity and electric conductivity).

This development opens the doors for many applications of the electrospray in high-value added technologies requiring flow rates that are manageable with up to $O(10^6-10^7)$ multiplexing of an individual electrospray source.

Acknowledgment

The support of the US Army under Cooperative Agreement no. W911NF-05-2-0015 (Dr. C. Mike Waits, Contract Monitor) is gratefully acknowledged.

References

- Bailey, A. G. (1988). *Electrostatic spraying of liquids*. UK: Research Studies Press.
- Bocanegra, R., De La Mora, J. F., & Gamero-Castaño, M. (2004). Ammonium electrolytes quench ion evaporation in colloidal propulsion. *Journal of Propulsion and Power*, 20, 728–735.
- Bocanegra, R., Galán, D., Márquez, M., Loscertales, I. G., & Barrero, A. (2006). Multiple electrospays emitted from an array of holes. *Journal of Aerosol Science*, 36, 1387–1399.
- Chen, D., Pui, D. Y. H., & Kaufman, S. L. (1995). Electro spraying of conducting liquids for monodisperse aerosol generation in the 4 nm to 1.8 μ m diameter range. *Journal of Aerosol Science*, 26, 963–977.
- Cloupeau, M., & Prunet-Foch, B. (1989). Electrostatic spraying of liquids in cone-jet mode. *Journal of Electrostatics*, 22(2), 135–159.
- Cloupeau, M., & Prunet-Foch, B. (1990). Electrostatic spraying of liquids: Main functioning modes. *Journal of Electrostatics*, 25(2), 165–184.
- Deng, W., & Gomez, A. (2007). Influence of space charge on the scale-up of multiplexed electrospays. *Journal of Aerosol Science*, 38, 1062–1078.
- Deng, W., & Gomez, A. (2008). Highly efficient integrated circuit cooling by multiplexed electrospays. In *AAAR 27th Annual Conference*, Orlando, FL, USA, October 20–24, 2008.
- Deng, W., Klemic, J. F., Li, X., Reed, M., & Gomez, A. (2006). Increase of electrospray throughput using multiplexed microfabricated sources for the scalable generation of monodisperse droplets. *Journal of Aerosol Science*, 37, 696–714.
- Deng, W., Klemic, J. F., Li, X., Reed, M., & Gomez, A. (2007). Liquid fuel combustor miniaturization via microfabrication. *Proceedings of the Combustion Institute*, 31, 2239–2246.
- Dole, M., Mack, L. L., Hines, R. L., Chemistry, D. O., Mobley, R. C., Ferguson, L. D. et al. (1968). Molecular beams of macroions. *Journal of Chemical Physics*, 49(5), 2240–2249.
- Duby, M.-H., Deng, W., Kim, K., Gomez, T., & Gomez, A. (2006). Stabilization of monodisperse electrospays in the multi-jet mode via electric field enhancement. *Journal of Aerosol Science*, 37, 306–322.
- Fenn, J. B., Mann, M., Meng, C. K., Wong, S. F., & Whitehouse, C. M. (1989). Electrospray ionization for mass spectrometry of large biomolecules. *Science*, 246(4926), 64–71.
- Fernández de la Mora, J., Navascues, J., Fernandez, F., & Rosell Llompart, J. (1990). Generation of submicron monodisperse aerosols by electrospays. *Journal of Aerosol Science*, 21(S1), s673–s676.
- Ganan-Calvo, A. M., Davila, J., & Barrero, A. (1997). Current and droplet size in the electro spraying of liquids: Scaling laws. *Journal of Aerosol Science*, 28(2), 249–275.
- Gomez, A. (2002). The electrospray and its application to targeted drug inhalation. *Respiratory Care*, 47, 1419.
- Gomez, A., Berry, J. J., Roychoudhury, S., Coriton, B., & Huth, J. (2007). From jet fuel to electric power using a mesoscale, efficient, Stirling system. *Proceedings of the Combustion Institute*, 31, 3251–3259.
- Gomez, A., Bingham, D., De Juan, L., & Tang, K. (1998). Production of protein nanoparticles by electrospray drying. *Journal of Aerosol Science*, 29(5–6), 561–574.
- Jaworek, A., & Sobczyk, A. T. (2008). Electro spraying route to nanotechnology: An overview. *Journal of Electrostatics*, 66(3–4), 197–219.
- Kelly, R. T., Page, J. S., Tang, K., & Smith, R. D. (2007). Array of chemically etched fused silica emitters for improving the sensitivity and quantitation of electrospray ionization mass spectrometry. *Analytical Chemistry*, 79(11), 4192–4198.
- Kim, J. S., & Knapp, D. R. (2001). Miniaturized multichannel electrospray ionization emitters on poly(dimethylsiloxane) microfluidic devices. *Electrophoresis*, 22, 3993–3999.
- Kim, W., Guo, M., Yang, P., & Wang, D. (2007). Microfabricated monolithic multinozzle emitters for nanoelectrospray mass spectrometry. *Analytical Chemistry*, 79, 3703–3707.
- Romero-Sanz, I., Bocanegra, R., Fernández de la Mora, J., & Gamero-Castaño, M. (2003). Source of heavy molecular ions based on Taylor cones of ionic liquids operating in the pure ion evaporation regime. *Journal of Applied Physics*, 94(5), 3599–3605.

- Rosell-Llompert, J., & Fernandez de la Mora, J. (1994). Generation of monodisperse droplets 0.3–4 μm in diameter from electrified cone-jets of highly conducting and viscous liquids. *Journal of Aerosol Science*, 25, 1093–1119.
- Rulison, A., & Flagan, R. C. (1993). Scale up of electro-spray atomization using linear arrays of Taylor cones. *Review of Scientific Instruments*, 64, 683–686.
- Salata, O. V. (2005). Tools of nanotechnology: Electro-spray. *Current Nanoscience*, 1, 25–33.
- Schaub, S., Alexander, D. R., & Barton, J. P. (1994). Theoretical analysis of the effects of particle trajectory and structural resonances on the performance of a phase-Doppler particle analyzer. *Applied Optics*, 33(3), 473–483.
- Tang, K., & Gomez, A. (1994a). Generation by electro-spray of monodisperse water droplets for targeted drug delivery by inhalation. *Journal of Aerosol Science*, 25(6), 1237–1249.
- Tang, K., & Gomez, A. (1994b). On the structure of an electrostatic spray of monodisperse droplets. *Physics of Fluids*, 6, 2317–2332.
- Tang, K., & Gomez, A. (1996). Monodisperse electro-sprays of low electric conductivity liquids in the cone-jet mode. *Journal of Colloid and Interface Science*, 184, 500–511.
- Tang, K., Lin, Y., Matson, D. W., Kim, T., & Smith, R. D. (2001). Generation of multiple electro-sprays using microfabricated emitter arrays for improved mass spectrometric sensitivity. *Analytical Chemistry*, 73(8), 1658–1663.
- Taylor, G. (1964). Disintegration of water drops in an electric field. *Proceedings of the Royal Society of London*, 280(1382), 383–397.
- Velásquez-García, L. F., Akinwande, A. I., & Martínez-Sánchez, M. (2006). A planar array of micro-fabricated electro-spray emitters for thruster applications. *Journal of Microelectromechanical Systems*, 15, 1272–1280.
- Waits, C. M., Morgan, B., Deng, W., Jankowski, N.R., Gomez, A., Geil, B. (2008). High density microfabricated multiplexed electro-spray. In *Proceedings of the 2008 solid-state sensor, actuator, and microsystems workshop (Hilton Head 2008)* (pp. 220–223), June 1–5, Hilton Head, South Carolina.
- Wang, L., Stevens, R., Malik, A., Rockett, P., Paine, M., Adkin, P. et al. (2007). High-aspect-ratio silica nozzle fabrication for nano-emitter electro-spray applications. *Microelectronic Engineering*, 84(5–8), 1190–1193.
- Zeleny, J. (1917). Instability of electrified liquid surfaces. *Physical Review*, 10, 1–6.